Direct numerical simulations of the turbulent mixing of a passive scalar

V. Eswaran and S. B. Pope
Sibley School of Mechanical and Aerospace Engineering, Cornell University, Ithaca, New York 14853

(Received 17 August 1987; accepted 30 November 1987)

The evolution of scalar fields, of different initial integral length scales, in statistically stationary, homogeneous, isotropic turbulence is studied. The initial scalar fields conform, approximately, to "double-delta function" probability density functions (pdf's). The initial scalar-to-velocity integral length-scale ratio is found to influence the rate of the subsequent evolution of the scalar fields, in accord with experimental observations of Warhaft and Lumley [J. Fluid Mech. **88**, 659 (1978)]. On the other hand, the pdf of the scalar is found to evolve in a similar fashion for all the scalar fields studied; and, as expected, it tends to a Gaussian. The pdf of the logarithm of the scalar-dissipation rate reaches an approximately Gaussian self-similar state. The scalar-dissipation spectrum function also becomes self-similar. The evolution of the conditional scalar-dissipation rate is also studied. The consequences of these results for closure models for the scalar pdf equation are discussed.

I. INTRODUCTION

Since their advent, direct numerical simulations[1] (DNS) have been established, along with the related large-eddy simulations (LES), as important tools of research in turbulent fluid mechanics. The introduction of bigger and faster computers has put turbulent flows with an ever-increasing range of Reynolds numbers within the grasp of these simulations.

Direct numerical simulations have been shown to be capable of accurately reproducing the physics of moderate-Reynolds-number turbulent flows (see, e.g., Refs. 2 and 3). These simulations use pseudospectral methods to solve the Navier–Stokes equation numerically without any modeling. Because of their accuracy, and the fact that almost complete information of the transient velocity and scalar fields is made available, these simulations are a powerful supplement to experimental investigations of turbulence phenomena.

Direct numerical simulations have been used to study different aspects of the behavior of scalars in homogeneous turbulence. Kerr[4] studies the small-scale structure of scalar fields. Herring and Kerr[5] used DNS to analyze the validity of two-point closure models like the direct interaction approximation. There have also been some simulation studies done on reactive flow problems.[6,7] The latter have been largely concerned with the effect of a decaying velocity field upon the rate of reaction of passive reactants in the flow. (Passive scalars are those that have no influence on the velocity field.)

The current DNS study of the mixing of an inert passive scalar in statistically stationary flows illuminates the process of turbulent mixing itself, without the added complications introduced by chemical reactions or by decaying turbulence. Also, simulations with decaying flow fields are often unduly influenced by the initial velocity fields because a significant amount of mixing occurs in the initial period of the simulation.

Situations that involve the advection and mixing of a scalar in a turbulent flow present an important class of problems to researchers of fluid flows. Instances of such problems appear, for example, in the analysis of chemically reactive flows, turbulent flames, and of pollutant dispersion in the atmosphere.

The difficulty of extracting information on the scalar field in turbulent flows has constrained experimental studies of this subject. However, a number of researchers have studied the evolution of one-point and two-point quantities of scalar fields in grid turbulence (see, e.g., Refs. 8 and 9). In these studies, the variance of the scalar has been shown (like the velocity variance) to decay in accordance with a power law in time (in a frame moving with the mean flow velocity). Warhaft and Lumley[8] have shown that the value of the exponent in the power law of the scalar-variance decay is dependent on the ratio of the wavenumbers at which the scalar and the velocity spectra peak. Antonopoulos-Domis[10] found that the scalar power-law exponent was essentially determined by the ratio of the initial dissipation microscales of the scalar and velocity fields in his large-eddy simulations of grid turbulence. Thus the length scales of the scalar and velocity fields play an important part in determining the turbulent mixing of the scalar. However, these studies focused on flows in which the velocity field was decaying. It is useful to know the extent to which the initial length scales of the scalar field influence the mixing process when the turbulence is statistically stationary. Another interesting point that arises is the question as to whether (and how rapidly) the scalar field reaches a self-similar state.

Research on turbulent mixing processes is of great interest to those working on turbulent-reactive flows. This is owing to the fact that turbulence causes the reactants in a flow to mix more rapidly and may thus significantly increase the rate of reaction, especially in the cases of relatively rapid chemical reactions where the mixing determines the overall rate. Probability density function (pdf) formulations have had some success in modeling reactive flow problems (see, e.g., Refs. 11 and 12). However, the molecular diffusion terms in the equation of the scalar pdf are unclosed and have to be modeled. Various closures have been proposed for this term in the one-point and two-point pdf equations.[13–18] However, little experimental evidence is available to confirm

 0031-9171/88/030506-15$01.90

the assumptions underlying these closures. It is, therefore, of interest to be able to study the character of the unclosed diffusion term so as to evaluate existing closures and, perhaps, propose new ones.

In the present work, direct numerical simulations are used to study decaying scalar fields in stationary, homogeneous turbulence. The initial scalar fields are constructed so that the scalar value at any point is close to either one of two specified values (i.e., conforming approximately to a "double-delta function" pdf). The simulations were performed so as to shed light on the following: (a) the effect of the initial length scales of the scalar field on the mixing process; (b) the evolution of the pdf's (and related quantities) of the scalar and the scalar-dissipation rate during the mixing process; and (c) the tendency of the scalar field to reach a self-similar state in the later stages of the decay.

Most of the simulations in this study were performed on a 64^3 grid, with a Taylor-scale Reynolds number of approximately 50 and a Prandtl number of 0.7. Among the quantities studied are the probability density functions of the scalar and the logarithm of the scalar-dissipation rate, the conditional scalar-dissipation rate, and the scalar-energy and scalar-dissipation spectrum functions.

In Sec. II the numerical method and the forcing scheme used in the simulations are briefly explained. In Sec. III an overview of the quantities considered in the simulations is given. Section IV describes the method used to generate the initial scalar fields. This is followed by the presentation of the results and a discussion of their significance in Sec. V. The paper closes with a summary of the most important conclusions in Sec. VI.

II. THE NUMERICAL METHOD AND FORCING SCHEME

A. The numerical method

The simulations were performed using a modified version of the computer code developed by Rogallo.[19] The code solves the continuity, Navier–Stokes, and scalar equations numerically on a three-dimensional grid.

The method of numerical solution is pseudospectral, i.e., the spatial-derivative terms in the Navier–Stokes and scalar equations are computed in spectral (Fourier) space, while the bilinear products in the convective terms are computed in physical space. The aliasing errors caused by the latter operations are almost completely removed by phase shifting and truncation techniques.[19] The time-stepping scheme is an explicit second-order Runge–Kutta method.

The solution is obtained on a cubical uniform mesh with N^3 grid points. In physical space, the cube is of side L and the grid points are located at $\mathbf{x} \equiv (l_1\Delta, l_2\Delta, l_3\Delta)$, where l_1, l_2, and l_3 are integers between 0 and $N-1$, and the grid spacing Δ is equal to L/N. The grid points (or nodes) in wavenumber space are at $\mathbf{k} \equiv (m_1k_0, m_2k_0, m_3k_0)$, where m_1, m_2, and m_3 are integers between $1-N/2$ and $N/2$ and k_0 (the lowest nonzero wavenumber) is equal to $2\pi/L$. The value of N is 64 for all simulations but one, for which it is 32.

The dependent variables in the simulations are the amplitudes of the discrete complex Fourier transforms, $\tilde{\mathbf{u}}(\mathbf{k},t)$ and $\Phi(\mathbf{k},t)$, of the velocity and scalar values at the grid points, $\mathbf{u}(\mathbf{x},t)$ and $\phi(\mathbf{x},t)$, respectively. The use of Fourier representation imposes periodic boundary conditions on the velocity and scalar fields, i.e.,

$$\mathbf{u}(\mathbf{x}+\mathbf{n}L,t) = \mathbf{u}(\mathbf{x},t), \tag{1}$$

and

$$\phi(\mathbf{x}+\mathbf{n}L,t) = \phi(\mathbf{x},t), \tag{2}$$

where $\mathbf{n}$ is any integer vector. Furthermore, the mean velocity is chosen to be zero, i.e., $\tilde{\mathbf{u}}(0,t) = 0$.

To obtain simulations that are well resolved and have acceptably small time-stepping errors, three conditions have to be satisfied.

(i) The highest wavenumbers in the computational box must be large enough to represent the smallest length scales in the flow (which are of the order of the Kolmogorov length scale, η). It was previously found that good resolution is obtained when the parameter $k_{\max}\eta$ is greater than or equal to unity,[20] where $k_{\max}$ is the maximum significant wavenumber resolved by the grid. The value of $k_{\max}$ is $\sqrt{2}Nk_0/3$ ($= 30.17k_0$ for 64^3 simulations): the factor $\sqrt{2}/3$ arises from the alias removal procedure used.

(ii) The integral length scale of the velocity field (to be defined later) must be sufficiently small (less than $L/3$, say) so that the periodic boundary conditions do not unduly constrain the solution.

(iii) The time step Δt must be sufficiently small. The parameter that is used to control the time-stepping errors is the nondimensional time step, the Courant number, which is defined by

$$C = (|u| + |v| + |w|)_{\max}\Delta t/\Delta, \tag{3}$$

where u, v, w are the components of velocity (in physical space) at a grid point. It is clear that, other things being the same, the choice of higher Courant numbers will decrease the computer time needed for a simulation. However, Courant numbers greater than unity are found to cause a marked increase in the time-stepping errors.[20] In the simulations in this study the Courant number is chosen to be 0.8.

B. The forcing scheme

In order to obtain statistically stationary velocity fields, the simulations are "forced," i.e., energy is added to the velocity field at low wavenumbers. This causes the simulations to reach a quasiequilibrium state where the energy dissipated at the small scales is equal to the energy added at the large scales.

The forcing scheme used is fully described and tested elsewhere.[20] Briefly, the forcing is done by including an additional term in (the spectral form of) the Navier–Stokes equation in a low-wavenumber band. Therefore, the equation determining the forced velocity field is

$$\frac{\partial\tilde{\mathbf{u}}(\mathbf{k},t)}{\partial t} = \tilde{\mathbf{a}}(\mathbf{k},t) + \mathbf{a}^f(\mathbf{k},t), \tag{4}$$

where $\tilde{\mathbf{a}}(\mathbf{k},t)$ is the Fourier transform of the rate of change of velocity with time, evaluated using the Navier–Stokes equation, and $\mathbf{a}^f(\mathbf{k},t)$ is the additional forcing acceleration. The forcing acceleration is nonzero only for wavenumbers $\mathbf{k}$ that satisfy $0 < |\mathbf{k}| \leqslant K_F$, where K_F is the maximum forcing wave-

number, chosen here to be $K_F = 2\sqrt{2}k_0$. At each of these wavenumbers, $\mathbf{a}^f(\mathbf{k},t)$ is obtained from a three-dimensional complex stochastic process, $\mathbf{b}(\mathbf{k},t)$, which is composed of six independent Uhlenbeck–Ornstien processes (see, e.g., Ref. 21), each with a time scale T_L, and standard deviation σ. In terms of $\mathbf{b}(\mathbf{k},t)$, $\mathbf{a}^f(\mathbf{k},t)$ is defined by

$$\mathbf{a}^f(\mathbf{k},t) = \mathbf{b}(\mathbf{k},t) - \mathbf{k}\mathbf{k}\cdot\mathbf{b}(\mathbf{k},t)/k^2, \tag{5}$$

which ensures that $\mathbf{a}^f(\mathbf{k},t)$ satisfies the continuity equation ($\mathbf{k}\cdot\mathbf{a}^f = 0$).

The forcing scheme introduces three nondimensional quantities in the simulations: the forcing Reynolds number, $\mathrm{Re}^*(\equiv\epsilon^{*1/3}k_0^{-4/3}/\nu)$, the nondimensional forcing time scale $T_L^*(\equiv T_L\epsilon^{*1/3}k_0^{2/3})$, and the nondimensional maximum forcing wavenumber K_F/k_0. Here ν is the kinematic viscosity and ϵ^* is defined by $\epsilon^* \equiv \sigma^2 T_L$. These three nondimensional quantities can be varied to obtain simulations of different Reynolds numbers and nondimensionalized Kolmogorov length scales ($k_0\eta$). For all the simulations in this study, K_F/k_0 is equal to $2\sqrt{2}$.

The forcing scheme used in this study has been shown to yield relatively isotropic velocity fields.[20] As homogeneity follows as a direct consequence of the numerical scheme, the velocity fields in this study are, therefore, homogeneous and isotropic.

III. CALCULATED QUANTITIES

The pdf's of the scalar, $\phi(\mathbf{x},t)$, and of the logarithm of the scalar-dissipation rate, $\epsilon_\phi(\mathbf{x},t)$ [$\equiv D\nabla\phi(\mathbf{x},t)\cdot\nabla\phi(\mathbf{x},t)$, where D is the diffusivity of the scalar], were computed at regular time-step intervals during the simulations. The pdf's were estimated by generating histograms, with a relatively large number of intervals (200), from the values of ϕ and ϵ_ϕ at the grid points. As there are about one-quarter of a million grid points (in a 64^3 simulation), the marginal pdf's can be expected to have low statistical errors. The pdf of $\ln(\epsilon_\phi)$ was calculated instead of the pdf of ϵ_ϕ because the latter pdf has a long "tail," which makes it difficult to estimate an appropriate upper bound to be used when constructing the histograms.

The conditional expectation of the scalar-dissipation rate,

$$\chi(\tilde{\phi},t) \equiv \langle \epsilon_\phi(\mathbf{x},t) | \phi(\mathbf{x},t) = \tilde{\phi} \rangle, \tag{6}$$

is a quantity of great interest because of its central role in the scalar pdf equation. For the case considered—a homogeneous scalar field in homogeneous turbulence—the scalar pdf, $P_\phi(\tilde{\phi};t)$, and indeed all one-point statistics, are independent of $\mathbf{x}$. The equation determining the evolution of $P_\phi(\tilde{\phi};t)$ can be written as[14]

$$\frac{\partial P_\phi(\tilde{\phi};t)}{\partial t} = -\frac{\partial^2}{\partial\tilde{\phi}^2}[\chi(\tilde{\phi},t)P_\phi(\tilde{\phi};t)]. \tag{7}$$

It may be seen then, for the homogeneous case, the sole unknown in the scalar pdf equation is the conditional dissipation $\chi(\tilde{\phi},t)$. Many closures have been proposed for the pdf equation,[13–18] few of which are based on a direct model for $\chi(\tilde{\phi},t)$.

The conditional expectation, $\chi(\tilde{\phi},t)$, is estimated by generating a histogram of the scalar values, $\phi(\mathbf{x},t)$, weighted by the corresponding scalar-dissipation rate, $\epsilon_\phi(\mathbf{x},t)$, at the same point. The values of this function at each interval is then divided by the (unweighted) histogram value of the scalar at the appropriate interval to yield the estimate of $\chi(\tilde{\phi},t)$. To decrease statistical errors, fewer histogram intervals (50) are used (compared to 200 used for estimating the pdf).

Among the other quantities computed are the energy, scalar-energy, and scalar-dissipation spectrum functions. The energy spectrum function $E(nk_0,t)$ and the scalar-energy spectrum function $E_\phi(nk_0,t)$ ($n = 0,1,2,\ldots,N_{\max}$), describe the energy and scalar energy in wavenumber shells of thickness k_0. (Here $N_{\max}$ is the greatest integer less than $k_{\max}/k_0$, which is 30 for a 64^3 grid.) The spectra are computed by summing the squares of the complex Fourier modes of velocity and scalar, respectively, for all $\mathbf{k}$, such that $nk_0 - k_0/2 \leqslant |\mathbf{k}| < nk_0 + k_0/2$. The scalar-dissipation spectrum function $D_\phi(nk_0,t)$ is similarly computed directly from the Fourier modes by summing $2Dk^2\Phi(\mathbf{k},t)\Phi^*(\mathbf{k},t)$ in each wavenumber shell. (The asterisk indicates the complex conjugate.)

[A technical detail, which is reported for completeness, is that the spectra are compensated for nonuniform node density. In the shell centered on nk_0 there are $M(n)$ nodes, and the node density is

$$M'(n) \equiv M(n)/\{\tfrac{4}{3}\pi[(n+\tfrac{1}{2})^3 - (n-\tfrac{1}{2})^3]\}. \tag{8}$$

This node density is approximately unity (i.e., independent of n); but, especially for small n, there are variations. To compensate for this nonuniformity, the spectrum functions are computed as described above and then divided by $M'(n)$.]

The volume-averaged scalar variance $\langle\phi^2\rangle$ is calculated from the scalar spectrum function, i.e.,

$$\langle\phi^2\rangle = k_0 \sum_{n=0}^{n=N_{\max}} E_\phi(nk_0). \tag{9}$$

[Because of the symmetry of the scalar values, $\langle\phi\rangle$ is zero, and $\langle\phi^2\rangle$ is equal to ϕ'^2, where ϕ' is the root-mean-square (rms) value of the scalar.] The volume-averaged scalar dissipation $\langle\epsilon_\phi\rangle$, defined by

$$\langle\epsilon_\phi\rangle \equiv D\langle\nabla\phi(\mathbf{x},t)\cdot\nabla\phi(\mathbf{x},t)\rangle = \frac{k_0}{2}\sum_{n=0}^{n=N_{\max}} D_\phi(nk_0), \tag{10}$$

is also computed.

Three length scales characterize the energy-containing scales, the dissipation scales, and the mixed energy-dissipation scales of the turbulent velocity fields. They are, respectively, the average integral scale

$$l \equiv \frac{1}{3}\sum_{i=1}^{i=3}\frac{\pi}{2u^2}E_{1i}(0,t), \tag{11}$$

the Kolmogorov microscale

$$\eta \equiv (\nu^3/\epsilon)^{1/4}, \tag{12}$$

and the Taylor microscale

$$\lambda \equiv (\epsilon/15\nu u^2)^{-1/2}, \tag{13}$$

where $E_{1i}(k,t)$ is the one-dimensional longitudinal energy

spectrum of the ith velocity component (see, e.g., Ref. 22), u is the rms value of the components of velocity, and ϵ is the volume-averaged energy-dissipation rate.

Each simulation is characterized by the Reynolds number based on the Taylor microscale, $\mathrm{Re}_\lambda \equiv u\lambda/\nu$, and the nondimensional Kolmogorov length scale, $k_0\eta$. Simulations that have the same values of these two parameters display nearly identical statistics for a number of quantities previously studied.[20]

We use the eddy-turnover time l/u to normalize the time t.

The two length scales of the scalar field considered here are the integral length scale l_ϕ, defined by

$$l_\phi \equiv (\pi/2\langle\phi^2\rangle)E_{1\phi}(0,t), \tag{14}$$

and the scalar dissipation scale λ_ϕ, defined by

$$\lambda_\phi \equiv [\,(\langle\epsilon_\phi\rangle/6D\,\langle\phi^2\rangle)\,]^{-1/2}, \tag{15}$$

where $E_{1\phi}(k,t)$ is the one-dimensional scalar-energy spectrum.

IV. INITIAL SCALAR FIELD

A. Initialization of the scalar fields

The initial scalar fields, $\phi(\mathbf{x},0)$, are constructed so that the pdf of the scalar values conforms as closely to a double-delta function as is allowed by the constraints imposed by the numerical scheme. That is, the scalar values of the initial fields are as close to either one of two values ($+1$ and -1, in this case) as is possible while keeping the fields smooth enough to be well-resolved in the simulations.

The procedure used to create these initial scalar fields is as follows.

(a) First, the Fourier amplitudes of the scalar field are assigned random values such that the resultant scalar-energy spectrum function is equal to a specified function, $f_\phi(k)$. The corresponding Fourier phases are randomly chosen. This is done by the following assignment:

$$\Phi(\mathbf{k},0) = [\,f_\phi(k)/4\pi k^2\,]^{1/2}\exp[2\pi i\theta(\mathbf{k})], \tag{16}$$

where (here and below) k is the magnitude of $\mathbf{k}$, and $\theta(\mathbf{k})$ is a uniformly distributed random number between 0 and 1 (chosen independently for each node). The function $f_\phi(k)$ is chosen to be a "top-hat" function, defined more precisely in the following subsection.

The scalar-energy spectrum function is computed from the relationship

$$E_\phi(nk_0,t) = \alpha\sum_{K_n}\Phi(\mathbf{k},t)\Phi^*(\mathbf{k},t), \quad n = 0,1,2,\ldots,N_{\max}, \tag{17}$$

where K_n is the set of all wavenumbers that satisfy $nk_0 - k_0/2 \leqslant |\mathbf{k}| < nk_0 + k_0/2$, and α is a normalization factor. Therefore, after the first step of the initialization, the scalar spectrum is

$$E_\phi(nk_0,t) = \alpha\sum_{K_n}\frac{f_\phi(k)}{4\pi k^2}, \tag{18}$$

where the left-hand side of the equation approximately equals the average value of $f_\phi(k)$ over the interval of summation.

(b) Next, the scalar field is (inverse-Fourier) transformed into physical space. In physical space, the scalar value at each node is reset to 1, if it is positive, and to -1 if it is negative. This operation yields the desired "double-delta" distribution but also causes the scalar value to change abruptly between adjacent nodes, thereby causing significant high-wavenumber components in the scalar field that are poorly resolved in the simulations.

(c) In the final step of the initialization the scalar field is retransformed into spectral space. The Fourier amplitudes of the scalar are multiplyed by a filter function, $F(\mathbf{k})$, defined by

$$F(\mathbf{k}) = \begin{cases} 1, & \text{if } k \leqslant k_c, \\ (k/k_c)^{-2}, & \text{if } k > k_c, \end{cases} \tag{19}$$

where k_c is a specified cutoff wavenumber. This filtering operation removes much of the poorly resolved high-wavenumber components of the scalar fields.

B. The length scale of the initial scalar field

As one of our stated aims is to observe the effect of the length scale of the initial scalar field upon the subsequent mixing, a systematic method of varying the length scale is needed. The method used simply consists of changing the function $f_\phi(k)$, which is used to create the initial scalar field.

The function $f_\phi(k)$ is chosen to be a "top-hat" function of width k_0, centered on a selected integer wavenumber k_s, i.e.,

$$f_\phi(k) = \begin{cases} 1, & \text{if } k_s - k_0/2 \leqslant k \leqslant k_s + k_0/2, \\ 0, & \textit{otherwise.} \end{cases} \tag{20}$$

The parameter k_s/k_0 essentially determines the integral length scale of the scalar field. Higher values of k_s/k_0 yield lower length scales for the scalar field and vice versa.

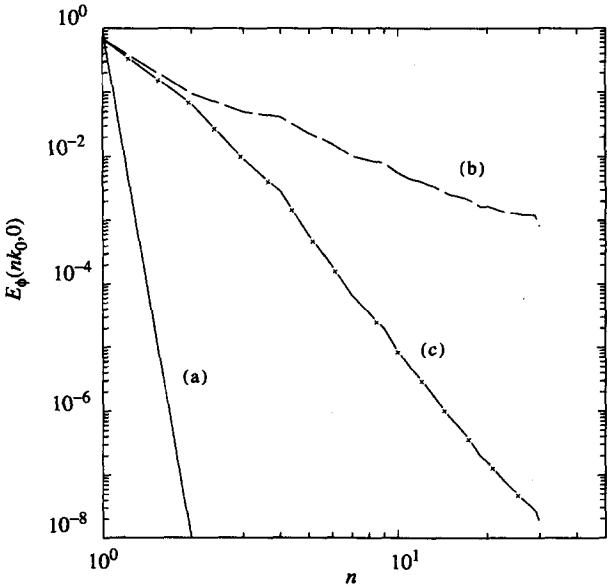

FIG. 1. The scalar-energy spectrum function at different stages in the scalar field initialization ($N = 64$, $k_s/k_0 = 1$, $k_c/k_s = 2$). The lines (a), (b), and (c) are the function after the respective initialization stages.

The second parameter in the specification of the initial scalar fields is the ratio k_c/k_s. For the same value of k_s, higher values of k_c allow more high-wavenumber scalar energy to exist after the creation of the initial scalar field. It is found, however, that this scalar energy is quickly eliminated by the high scalar dissipation in the high-wavenumber regions. This means that, beyond a certain limit, increasing k_c/k_s affects only the smaller scales where the consequent variation is short-lived.

Figure 1 shows the scalar-energy spectrum function at the end of steps (a), (b), and (c) of the initialization for a typical simulation with $k_s/k_0 = 1$ and $k_c/k_s = 2$. [In Fig. 1, the scalar-energy spectrum function at the end of stage (a) of the initialization is zero everywhere except at $n = 1$. For convenience in plotting the graph, 10^{-8} is used as a nominal zero.]

Figures 2 and 3 illustrate the influence of the cutoff wavenumber k_c. Figure 2 shows the scalar-dissipation spectra for the case $k_s/k_0 = 8$, with two different values of the cutoff: $k_c/k_0 = 2$ and 4. A little after the initialization [Fig. 2(a)] the difference is evident, but after about one-quarter of an eddy-turnover time [Fig. 2(b)] the two spectra are very similar—the high-wavenumber variation has been virtually eliminated. Figures 3(a) and 3(b) show the pdf of the logarithm of the scalar dissipation for the same cases shown in Figs. 2(a) and 2(b), respectively. Again, the two pdf 's in Fig. 3(b) are close to identical.

From this evidence we conclude that the effect of the parameter k_c/k_s (as long as it is not too small) is not significant beyond a short time from the scalar field initialization.

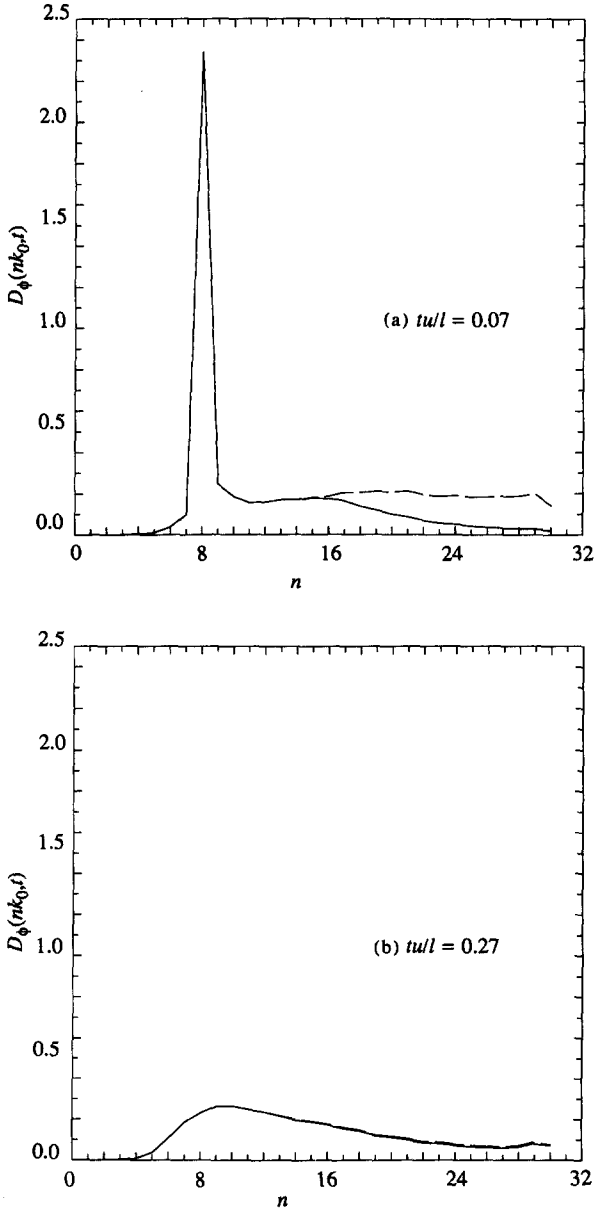

FIG. 2. The scalar-dissipation spectrum function for two simulations (F2e) with identical initial conditions ($k_s/k_0 = 8$), but different scalar-cutoff wavenumbers ($k_c/k_s = 2$ and 4, for the solid and dashed lines, respectively): (a) shortly after initialization ($tu/l = 0.07$); (b) a later time ($tu/l = 0.27$).

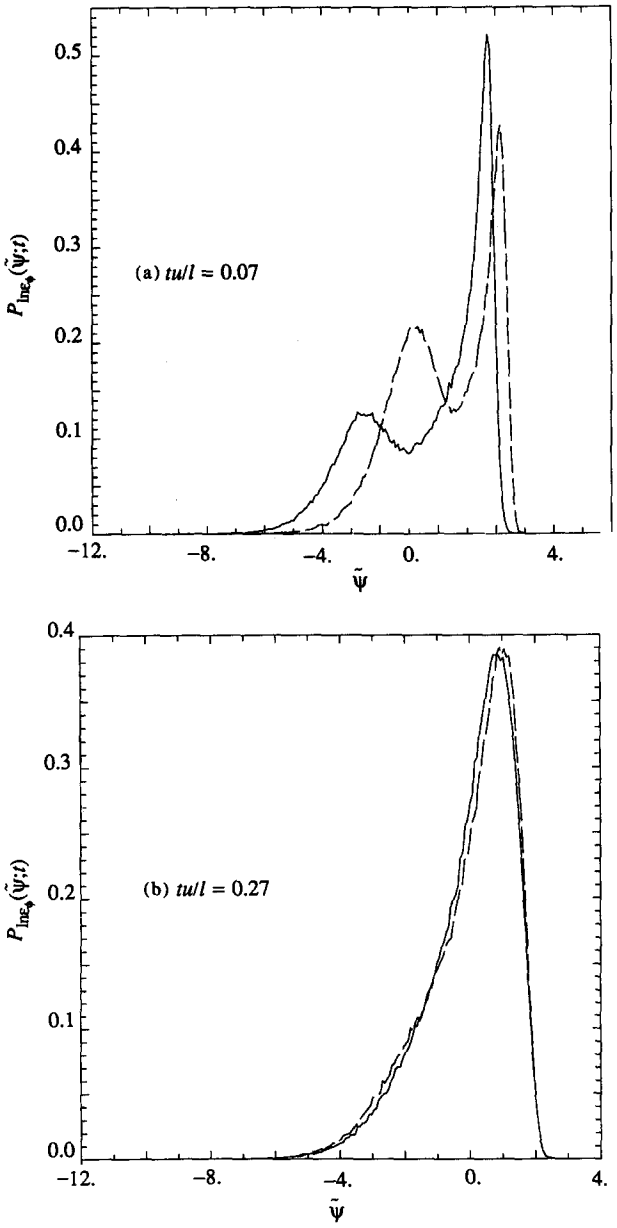

FIG. 3. The pdf 's of the logarithm of the scalar-dissipation rate for the same conditions as Fig. 2.

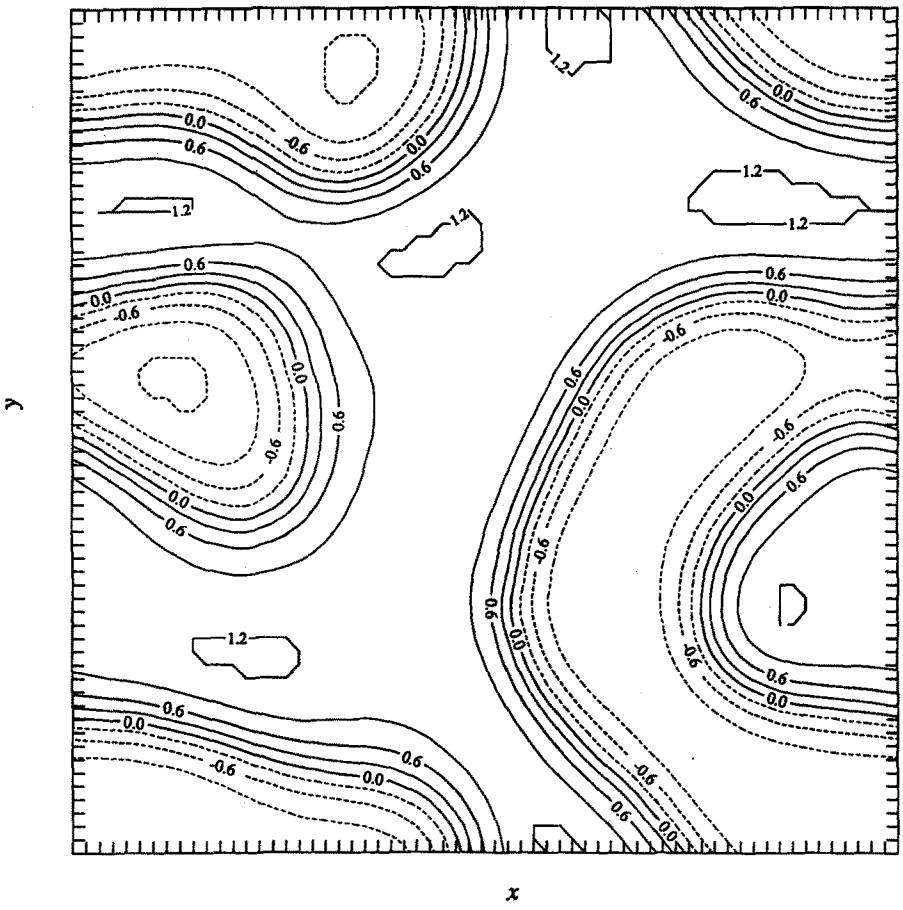

FIG. 4. Contour plot of the scalar values on an arbitrary plane in an initial scalar field. The contour interval is 0.3 ($k_s/k_0 = 1$; $k_c/k_s = 2$).

The value of k_c/k_s was chosen to be 2 for the simulations in this work. With this relatively small value we find that the scalar field is adequately resolved, even at early times.

Figure 4 shows the contour lines describing the initial scalar values on an arbitrary plane in a typical simulation ($k_s/k_0 = 1$). The solid and dashed lines indicate positive and negative scalar values, respectively. It can be seen that the initial scalar field consists of relatively broad patches where the scalar values are close to ± 1, which are separated by narrow transition zones with intermediate values.

The initial scalar pdf 's (and those at early times) may be seen in the figures presented below (e.g., Figs. 6 and 14–16).

C. Resolution of the scalar fields

It has been shown previously[20] that the velocity fields are, for most purposes, well-resolved when the parameter $k_{\max}\eta$ is greater than, or equal to, unity. In the simulations in this study, the lowest value of this parameter is 1.01 (simulations F2a–F2e; see Table I). It is necessary to show that the scalar fields are well-resolved at this value of $k_{\max}\eta$ for the Prandtl number of 0.7 used in this study.

This is done by comparing a simulation with a higher value of $k_{\max}\eta$ (1.42; simulation F3e) with another simulation with identical values for the other parameters, and with identical initial conditions, but with a value of $k_{\max}\eta$ equal to 1.01 (F3f). The maximum wavenumber, $k_{\max}$, was reduced in the latter simulation by discarding the Fourier modes outside a shell of the appropriate wavenumber when time stepping the solution of the Navier–Stokes and scalar equations.

Figures 5(a) and 5(b) show the evolution of the scalar rms and the scalar-dissipation rates from these two simulations. Except for a small difference in the scalar-dissipation rates during the initial period of the simulations, the results

TABLE I. Summary of forced turbulence simulations: velocity fields.

Run	Vel. field	$k_0\eta$	$k_{\max}\eta$	$k_0 l$	$k_0\lambda$	l/u	$T_R u/l$	Re_λ	D^*
F1a	v1	0.0376	1.13	1.17	0.528	0.49	3.9	50.5	0.581
F1c	v2	0.0368	1.11	1.02	0.510	0.42	4.4	49.9	0.590
F2a–F2e	v3	0.0359	1.01	1.01	0.464	0.38	4.4	49.2	0.663
F3a–F3e	v4	0.0473	1.42	1.11	0.583	0.66	4.2	39.2	0.664
F3f	v4	0.0473	1.01	1.11	0.583	0.67	4.2	39.2	0.664
F4[a]	v5	0.0721	1.09	1.24	0.744	1.34	14.2	27.6	0.730

[a] 32^3 simulation.

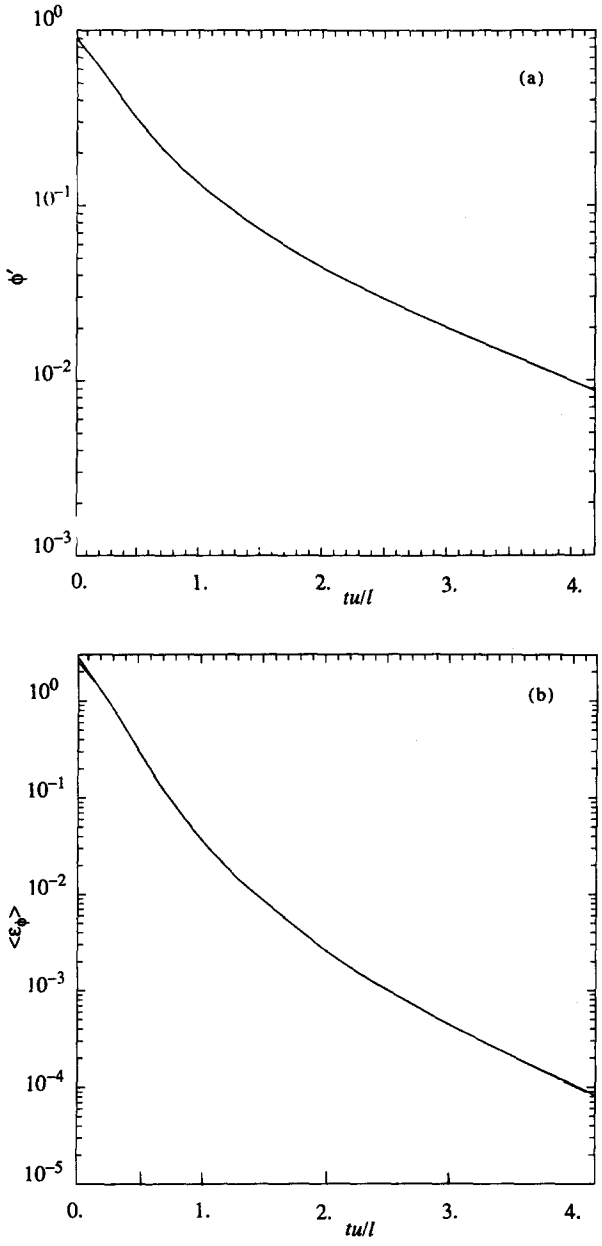

FIG. 5. The evolution of the scalar rms and dissipation rate for two simulations (F3e and F3f) with identical initial conditions, but different values of $k_{max}\eta$ (= 1.42 and 1.01, for the solid and dashed lines, respectively). The time is normalized by the eddy-turnover time ($Re_\lambda \approx 40$): (a) the scalar rms (the two lines are indistinguishable); (b) the scalar-dissipation rate.

are identical for the two cases. This evidence strongly suggests that the scalar fields are well-resolved for simulations with a value of $k_{max}\eta$ of at least 1.01 and a Prandtl number of 0.7.

V. RESULTS

This section contains the results obtained from a series of direct numerical simulations of the turbulent mixing of a passive scalar in statistically stationary turbulence. The initial scalar fields have a prescribed integral length scale and the initial pdf of the scalar conforms roughly to a double-delta function distribution.

The initial velocity fields are generated by running (pre) simulations, starting from (almost) arbitrary initial conditions and with prescribed forcing parameters (Re*, T_L^* and K_F/k_0) for four or more eddy-turnover times. Statistical stationarity is reached by the end of these computer runs. The velocity fields are stored and used as the initial velocity fields for the simulations.

A. Flow conditions

The principal parameters and output quantities from the simulations in this study are presented in Tables I and II. The symbols v1,v2,... and s1,s2,..., etc., in these tables refer to different initial velocity and scalar fields, respectively, T_R refers to the real time of a simulation, and D^* is the nondimensional energy-dissipation rate ($D^* \equiv \epsilon/u^3 k_0$).

The 64^3 simulations were performed for Reynolds numbers of, approximately, 40 and 50 (corresponding to a nondimensional Kolmogorov length scale of $k_0\eta \approx 0.047$ and 0.037, respectively). The forcing Reynolds number Re* and time scale T_L^* are 9.421 and 0.15 ($Re_\lambda \approx 40$; simulations F3a–F3f) and 14.402 and 0.15 ($Re_\lambda \approx 50$; simulations F1a, F1c, F2a–F2e). The parameter K_F/k_0 is $2\sqrt{2}$ in all the simulations and the kinematic viscosity ν, and the Prandtl number Pr, are 0.025 and 0.7, respectively.

B. Statistical variability

When two or more simulations are performed with identical parameters (Re*, T_L^*, k_s/k_0, etc.) but with different random numbers used in the specification of the initial conditions, then some statistical variability between the simulations is expected.

In order to gauge the extent of this variability, three simulations (F1a, F1c, F2a) with identical parameters, but with different initial velocity and scalar fields, were studied. Figure 6 shows the initial pdf of the scalar for these simulations. The pdf 's are quite similar, although some variability is evident, not only from the differences between the curves, but also from the asymmetry of the pdf 's. Little variability is evident in the initial scalar-energy spectrum functions which are displayed in Fig. 7.

The evolution of the scalar rms ϕ', and the scalar dissipation $\langle\epsilon_\phi\rangle$ in Figs. 8 and 9, respectively, follow similar but

TABLE II. Summary of simulations: scalar fields.

Run	Scalar field	k_s/k_0	$(l_\phi/l)_{t=0}$	$(\lambda_\phi/\lambda)_{t=0}$
F1a	s1	1	1.248	3.28
F1c	s2	1	1.520	3.56
F2a	s3	1	1.484	3.83
F2b	s4	2	0.684	2.04
F2c	s5	4	0.450	1.07
F2d	s6	6	0.252	0.71
F2e	s7	8	0.182	0.54
F3a	s8	1	1.284	2.93
F3b	s9	2	0.544	1.62
F3c	s10	4	0.394	0.85
F3d	s11	6	0.242	0.56
F3e	s12	8	0.166	0.43
F3f	s12	8	0.168	0.44

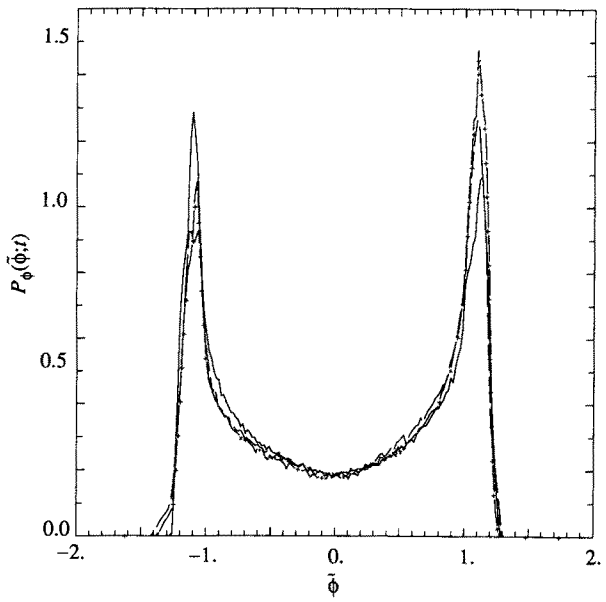

FIG. 6. The initial scalar pdf's for three simulations with identical input parameters but different initial conditions: F1a (dashed line), F1c (dashed line with pluses), and F2a (solid line) ($\mathrm{Re}_\lambda \approx 50$).

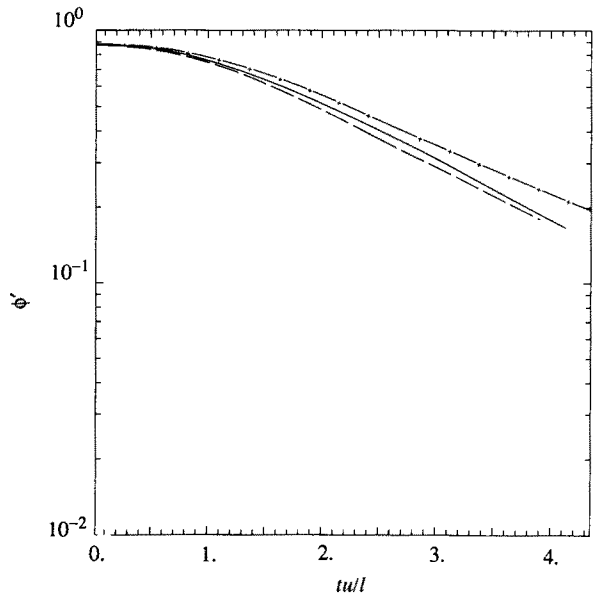

FIG. 8. The evolution of the scalar rms for the same cases as in Fig. 6.

not identical paths. This evidence suggests that the evolution of the scalar is, to a degree, sensitive to statistical variations in the initial scalar and velocity fields even when the relevant initial length scales are relatively unchanged (as in simulations F1c and F2a).

C. Evolution of scalar variance and dissipation

Figure 10 shows the decay of the scalar rms ϕ' for the five simulations F2a–F2e. In each case the velocity field is the same ($\mathrm{Re}_\lambda = 49.2$), but the initial scalar fields have different integral length scales l_ϕ—differing by as much as a factor of 8. It is clear from the figure that l_ϕ has a major effect on the decay rate, at least for the first two eddy-turnover times.

Figure 11, which shows the evolution of the scalar dissipation $\langle \epsilon_\phi \rangle$, explains the trends observed above. It is readily shown from an examination of the initialization procedure that (all other things being fixed) $\langle \epsilon_\phi \rangle$ is initially proportional to k_s^2 and hence to l_ϕ^{-2}. Thus, for example, the initial value of $\langle \epsilon_\phi \rangle$ for run F2e ($k_s/k_0 = 8$) is observed to be four times that of run F2c ($k_s/k_0 = 4$). For the two smallest initial values of l_ϕ (F2d and F2e), $\langle \epsilon_\phi \rangle$ may be seen to decay monotonically, whereas with the larger initial values of l_ϕ, $\langle \epsilon_\phi \rangle$ increases to a maximum before decaying.

In decaying grid turbulence, ϕ' and $\langle \epsilon_\phi \rangle$ decay with time according to power laws.[8] This corresponds to the me-

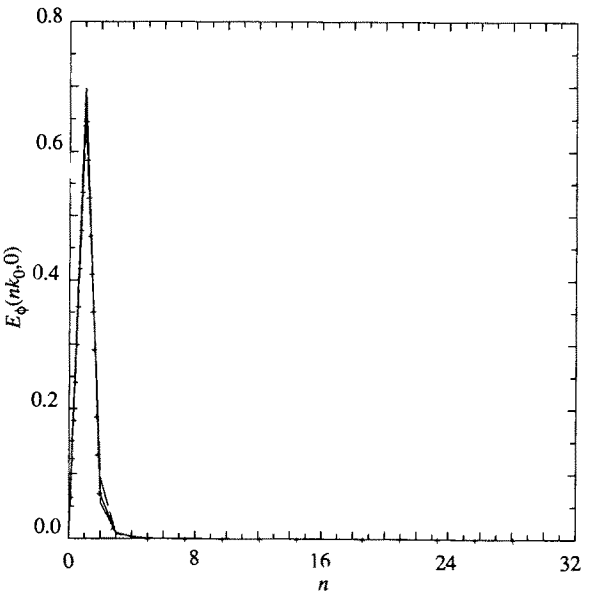

FIG. 7. The initial scalar-energy spectrum functions for the same cases as in Fig. 6.

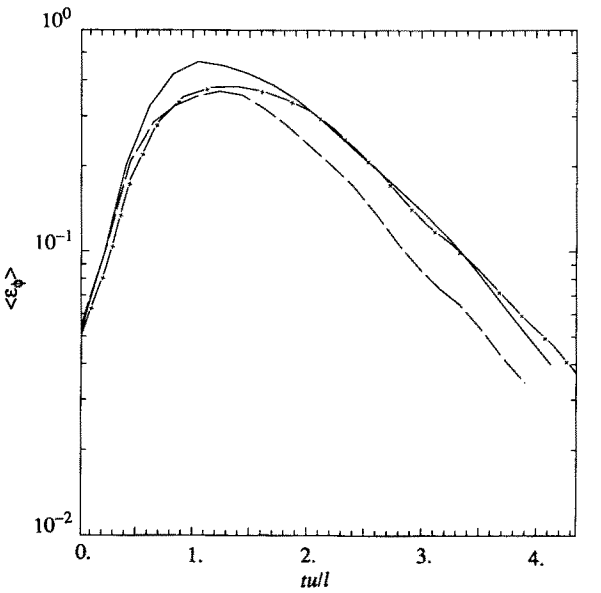

FIG. 9. The evolution of the scalar-dissipation rate for the same cases as in Fig. 6.

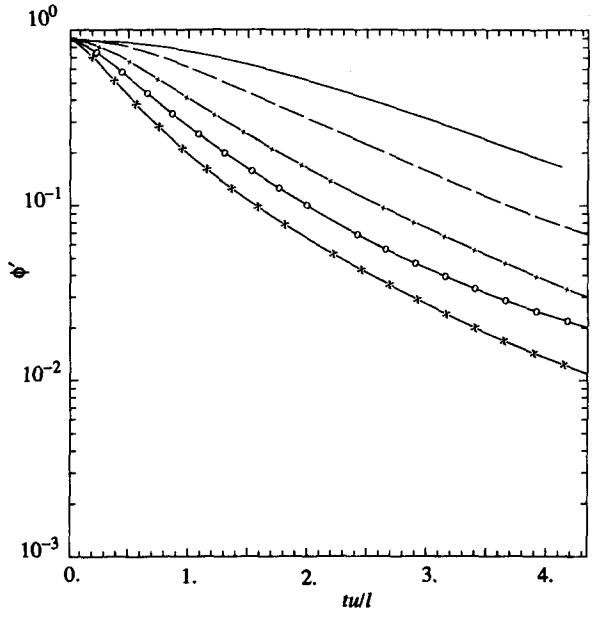

FIG. 10. The evolution of the scalar rms for simulations with identical initial velocity fields, but with different values of k_s/k_0. Data from simulations F2a (—; $k_s/k_0 = 1$), F2b (- - -; 2), F2c (- + -; 4), F2d (-o-; 6), and F2e (-x-; 8). The time is normalized by the eddy-turnover time ($\mathrm{Re}_\lambda \approx 50$).

chanical-to-scalar time-scale ratio

$$r \equiv (\langle \epsilon_\phi \rangle / \langle \phi^2 \rangle) / [\epsilon/(3u^2)], \tag{21}$$

being constant. Depending on the initial conditions, values of r in the range 0.6–2.4 are observed.[8,23] For the present case of forced stationary turbulence, a constant value of r results in exponential decay of ϕ' and $\langle \epsilon_\phi \rangle$. With the scales used in Figs. 10 and 11, exponential decay corresponds to lines of constant slope. The figures suggest that at large times ($t > 3l/u$, say) such constant-slope segments occur.

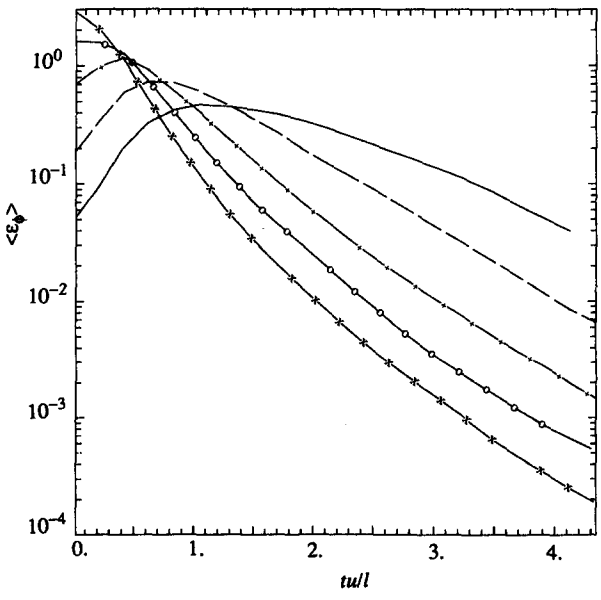

FIG. 11. The evolution of the scalar-dissipation rate for the same cases as in Fig. 10.

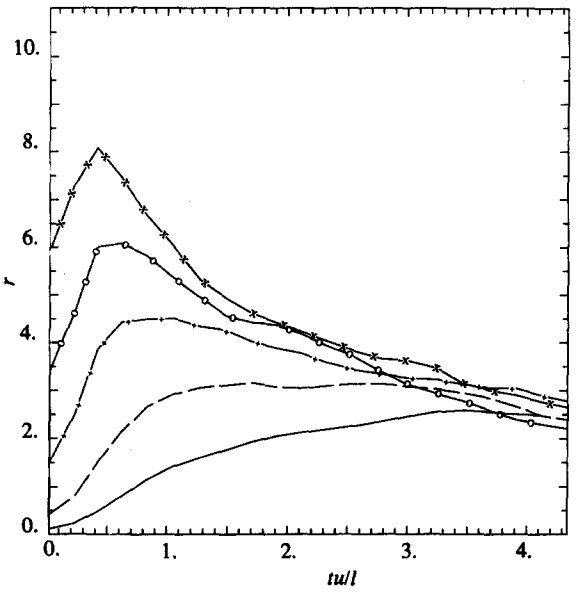

FIG. 12. The evolution of the mechanical-to-scalar time-scale ratio r for the same cases as in Fig. 10.

The question is addressed more directly by Fig. 12, which shows the evolution of r itself for the same five simulations. Like $\langle \epsilon_\phi \rangle$, initially r is proportional to l_ϕ^{-2}, all else being equal. In all cases, r rises initially but then levels off or decreases. Having initially differed by as much as a factor of 64, by $t = 4l/u$ the values of r are within 25% of each other, and several of the curves have crossed. This strongly suggests a trend toward a universal value independent of the initial condition. At the end of the simulations ($t = 4.4l/u$) the value of r is approximately 2.5, but a downward trend is still evident.

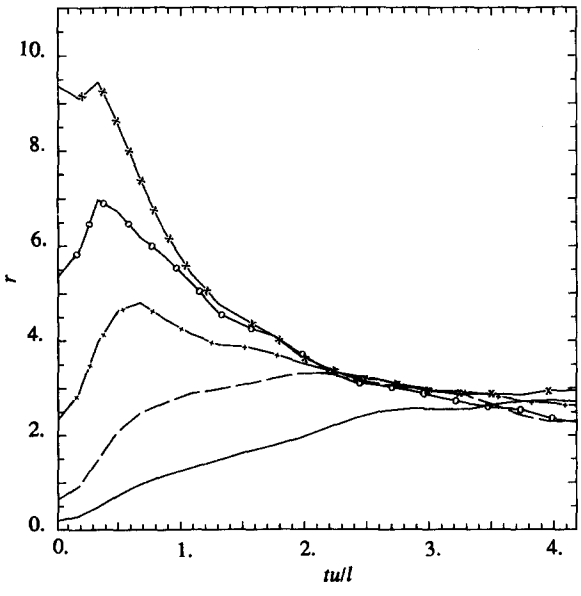

FIG. 13. The evolution of the mechanical-to-scalar time-scale ratio r for the simulations with $\mathrm{Re}_\lambda \approx 40$. Data from simulations F3a (—; $k_s/k_0 = 1$), F3b (- - -; 2), F3c (- + -; 4), F3d (-o-; 6), and F3e (-x-; 8). The time is normalized by the eddy-turnover time.

Simulations were also performed at a lower Reynolds number, $\mathrm{Re}_\lambda = 39.2$ (F3a–F3e). In all respects the results are analogous to those already reported. For example, Fig. 13 shows a similar evolution of the time-scale ratio r (cf. Fig. 12).

Our observation that r appears to approach a universal value independent of initial conditions is at variance with Warhaft and Lumley's observation.[8] This is discussed further in the next section.

D. Evolution of the scalar pdf

It is generally assumed that the scalar pdf $P_\phi(\tilde{\phi};t)$, starting from a double-delta function distribution, evolves towards a Gaussian. But the shapes adopted by $P_\phi(\tilde{\phi};t)$ during this evolution have hitherto been unknown.

For one simulation (F2a; $\mathrm{Re}_\lambda = 49.2$, $k_s/k_0 = 1$), Fig. 14 shows the scalar pdf $P_\phi(\tilde{\phi};t)$ at five different stages of its evolution. At the earliest time shown ($t = 0.22l/u$) little decay has taken place (see Fig. 10): the rms ϕ' is still 99% of its initial value, denoted by ϕ_0. The pdf at this early time has peaks close to $+1$ and -1 corresponding to unmixed fluid, and in between a U-shaped distribution. This is the expected contribution from diffusive layers, possibly with error function profiles of ϕ.

At the next time shown ($t = 1.49l/u$, $\phi' = 0.73\phi_0$) the peaks have disappeared, and the distribution is remarkably flat. Later still ($t = 2.11l/u$, $\phi' = 0.55\phi_0$) the pdf resembles an inverted parabola with a noticeable lack of tails. As time progresses further, the pdf evolves towards the familiar bell-shaped curve. In Sec. V F evidence is presented showing that the asymptotic shape is indeed Gaussian.

Remarkably, and importantly, the evolution of pdf shapes described above appears to be independent of the initial conditions. Figures 15 and 16 show $P_\phi(\tilde{\phi};t)$ for the cases

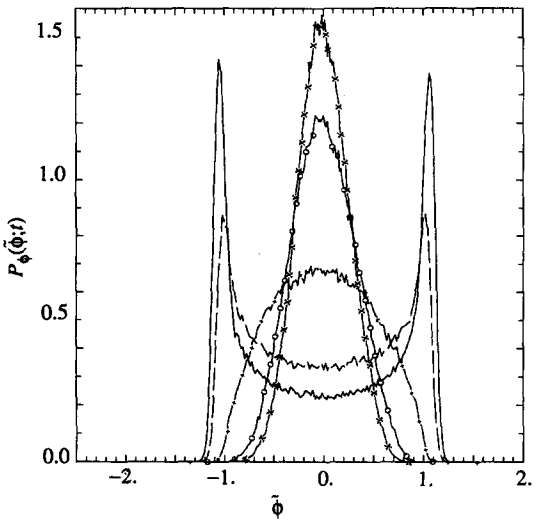

FIG. 15. The scalar pdf from simulation F2c ($\mathrm{Re}_\lambda \approx 50$, $k_s/k_0 = 4$) at different times. Lines: — ($tu/l = 0.22$; $\phi'/\phi_0' = 0.92$), - - - (0.42; 0.80), - + - (0.83; 0.54), -o- (1.28; 0.35), -x- (1.49; 0.28).

$k_s/k_0 = 4$ and 8, respectively. Thus while (as shown by Warhaft and Lumley[8]) l_ϕ/l is an important parameter in determining the rate of evolution of the scalar variance, it does not affect the shapes adopted by the scalar pdf. Needless to say, this observation greatly simplifies the task of constructing models for the evolution of scalar pdf 's. Also, even though our simulations are for particular initial conditions, the results have generality.

Figure 17 shows the evolution of the pdf of $\ln(\epsilon_\phi)$ for the simulation with the smallest initial scalar integral scale (F2e; $\mathrm{Re}_\lambda = 49.2$, $k_s/k_0 = 8$). Except at the first time shown, the pdf 's have a similar shape: they are bell shaped, with a slight negative skew (see Fig. 24 below). As time progresses, the pdf 's become centered on smaller values of $\ln(\epsilon_\phi)$, reflecting the decrease of $\langle \epsilon_\phi \rangle$ (see Fig. 11). At the

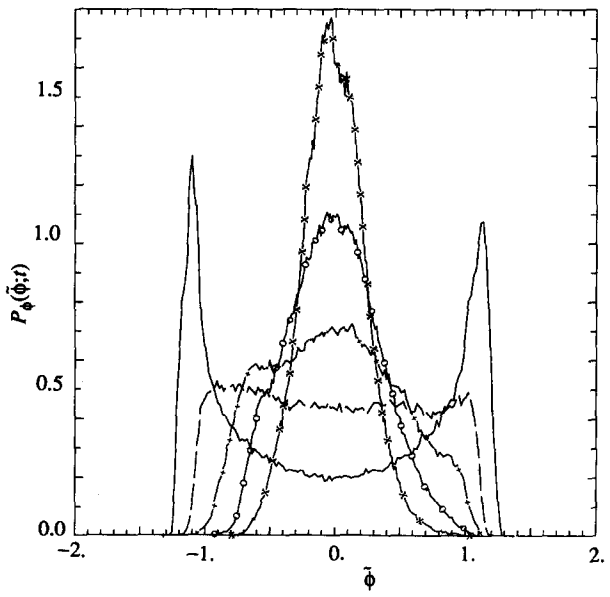

FIG. 14. The scalar pdf from simulation F2a ($\mathrm{Re}_\lambda \approx 50$, $k_s/k_0 = 1$) at different times. Lines: — ($tu/l = 0.22$; $\phi'/\phi_0' = 0.99$), - - - (1.49; 0.73), - + - (2.11; 0.55), -o- (2.78; 0.40), -x- (3.47; 0.27).

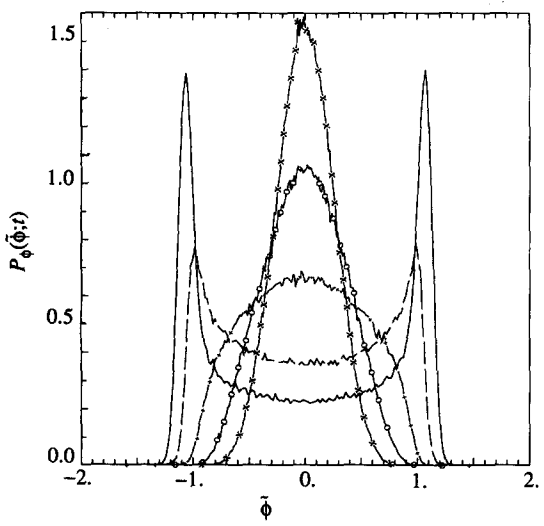

FIG. 16. The scalar pdf from simulation F2e ($\mathrm{Re}_\lambda \approx 50$, $k_s/k_0 = 8$) at different times. Lines: — ($tu/l = 0.07$; $\phi'/\phi_0' = 0.94$), - - - (0.22; 0.76), - + - (0.42; 0.54), -o- (0.62; 0.38), -x- (0.83; 0.27).

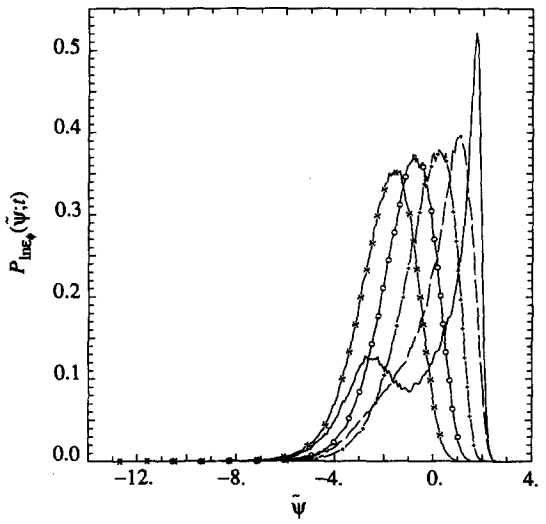

FIG. 17. The pdf of the logarithm of the scalar-dissipation rate for the same case as in Fig. 16.

earliest time, there is a significant probability of relatively very low dissipation, corresponding to fluid in unmixed blobs with $\phi \approx \pm 1$.

E. Conditional scalar dissipation

The pdf evolution equation [Eq. (7)] shows that, for the case considered, the scalar pdf $P_\phi(\tilde{\phi};t)$ evolves solely because of the effects of conditional scalar dissipation, $\chi(\tilde{\phi},t) = \langle \epsilon_\phi(\mathbf{x},t) | \phi(\mathbf{x},t) = \tilde{\phi} \rangle$. Figures 18 and 19 show for two simulations ($\mathrm{Re}_\lambda = 49.2$, $k_s/k_0 = 4$ and 8, respectively) the conditional scalar dissipation (normalized by the unconditional mean) at three times. At the first time shown (corresponding to $\phi' \approx 0.5\phi_0$) $\chi(\tilde{\phi},t)$ exhibits a parabolic shape, being maximum at $\tilde{\phi} = 0$, and small for large values of $|\tilde{\phi}|$. This is the expected shape for a field consisting of diffusive layers separating regions of approximate homogeneity.

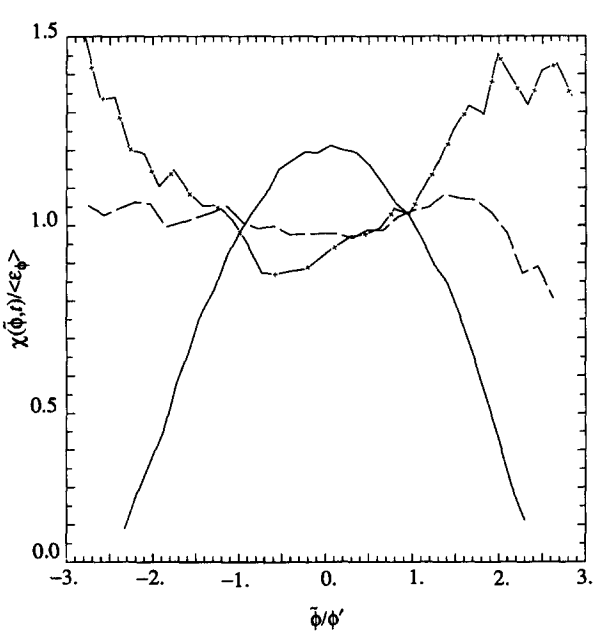

FIG. 18. The evolution of the conditional scalar-dissipation rate from simulation F2c ($\mathrm{Re}_\lambda \approx 50$, $k_s/k_0 = 4$). Lines: — ($tu/l = 1.05$; $\phi'/\phi_0' = 0.43$), - - - (2.11; 0.16), - + - (3.25; 0.07).

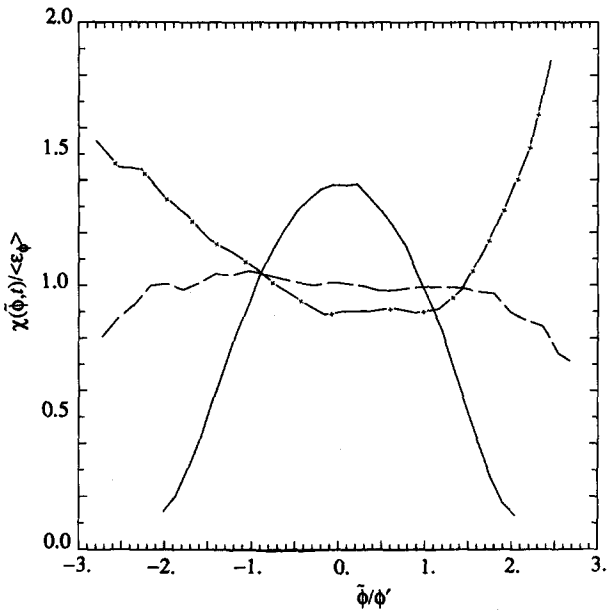

FIG. 19. The evolution of the conditional scalar-dissipation rate from simulation F2e ($\mathrm{Re}_\lambda \approx 50$, $k_s/k_0 = 8$). Lines — ($tu/l = 0.42$; $\phi'/\phi_0' = 0.54$), - - - (1.05; 0.20), - + - (2.78; 0.04).

At the intermediate time shown (corresponding to $\phi' \approx 0.2\phi_0$) the curves of $\chi(\tilde{\phi},t)$ appear almost flat, while at the latest time ($\phi' \approx 0.05\phi_0$) they are again parabolic but with a minimum at $\tilde{\phi} = 0$.

To examine further the dependence of ϵ_ϕ on ϕ, we consider the correlation function defined by

$$\rho = \langle \phi^2 \epsilon_\phi \rangle / (\langle \phi^2 \rangle \langle \epsilon_\phi \rangle) - 1. \tag{22}$$

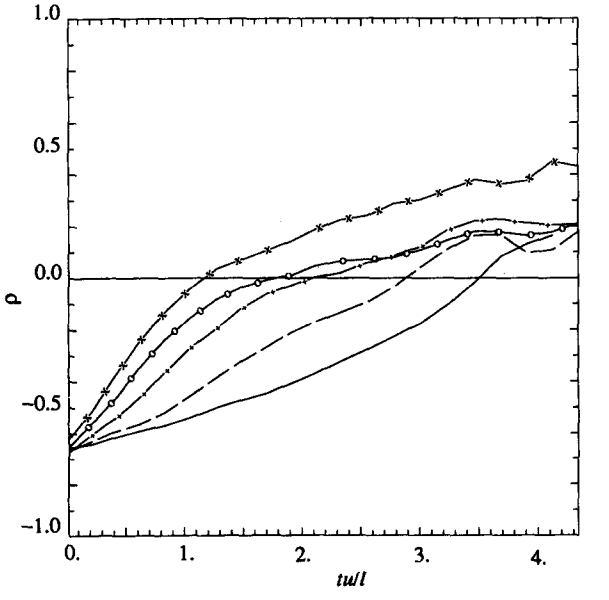

FIG. 20. The evolution of the scalar variance dissipation correlation function for simulations with identical initial velocity fields, but with different values of k_s/k_0. Data from simulations F2a (—; $k_s/k_0 = 1$), F2b (- - -; 2), F2c (- + -; 4), F2d (-o-; 6), and F2e (-x-; 8). The time is normalized by the eddy-turnover time ($\mathrm{Re}_\lambda \approx 50$).

This is not a correlation coefficient, but it has similar properties and is easier to evaluate accurately. If ϕ and ϵ_ϕ are independent, then ρ is zero. If large values of ϕ^2 are accompanied by large values of ϵ_ϕ, then ρ is positive, etc. Figure 20 shows the evolution of ρ with time for the five simulations with $\mathrm{Re}_\lambda = 49.2$. In all cases, ρ is initially about -0.65 and subsequently increases, most rapidly for the case with the smallest length scale. Eventually ρ becomes positive. It is shown below that for very large times, ρ asymptotes to zero, but this is not evident within the duration of these simulations.

The results for the simulations with $\mathrm{Re}_\lambda = 39.2$ (not shown) are similar in all respects.

F. Self-similarity at large times

We now address the following questions: at large times, does the scalar pdf become self-similar, independent of the initial conditions? And, if so, is the pdf Gaussian? It has already been observed that the evolution to an asymptotic state (assuming it to exist) is quite slow. For example, even after four eddy-turnover times, the time scale r is still evolving (see Fig. 12).

Figure 21 shows, for one simulation, the standardized scalar pdf at five late times ($\phi'/\phi_0 < 0.25$). (The standardized pdf is the pdf of ϕ/ϕ'.) It may be seen that there is fairly close agreement between the pdf's, although some differences are noticeable around the peak. The corresponding standardized pdf's of scalar dissipation are shown in Fig. 22. Again close agreement is observed.

Figure 23 shows the normalized scalar dissipation spectrum function at the end of the five simulations with $\mathrm{Re}_\lambda = 49.2$. Even though the initial spectra are quite different—the length scales differing by as much as a factor of 8—it may be seen that there is relaxation to a universal spectrum.

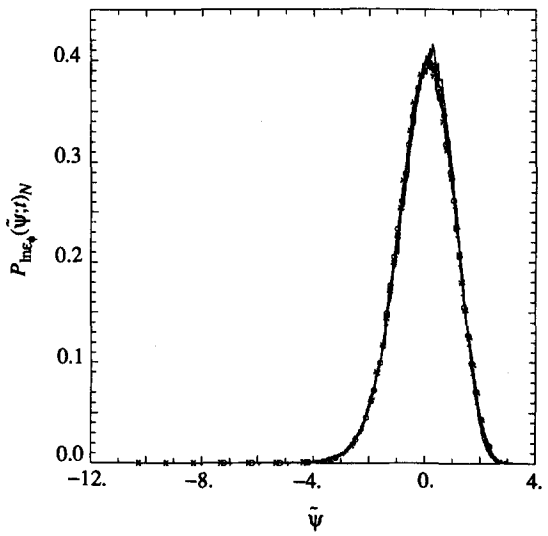

FIG. 22. The standardized pdf of the logarithm of the scalar-dissipation rate for the same case as in Fig. 21.

To examine more quantitatively the asymptotic form of the pdf's, the skewness and flatness factors of ϕ and $\ln(\epsilon_\phi)$ are shown in Fig. 24 for the simulation F2c. (Here $S_m[q]$ denotes the mth standardized central moment of the random variable q.) The skewness of $\ln(\epsilon_\phi)$ appears to reach a value of about -0.3, while the flatness reaches about 3.2. Thus ϵ_ϕ is not precisely log normal, though it is approximately so.

The skewness of ϕ is initially zero, but a small positive value develops. This can only be a result of statistical variability because in all respects ϕ is statistically symmetric about zero. The flatness starts slightly above 1 (the value for a double-delta distribution), passes through 3 (the Gaussian

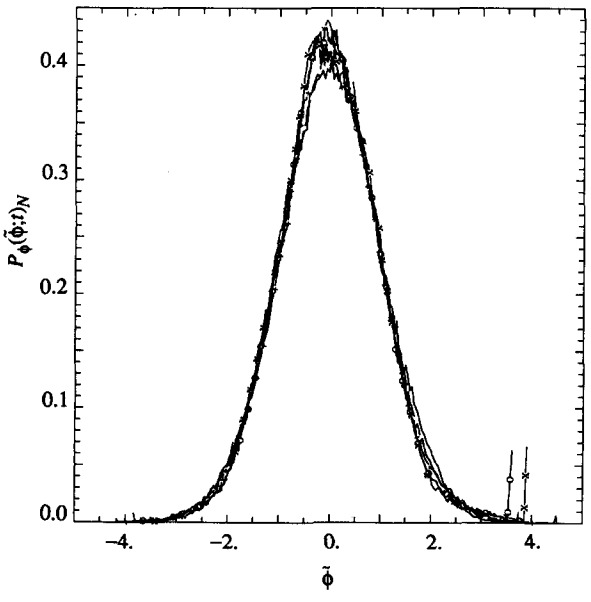

FIG. 21. The standardized pdf of the scalar at different times in the later period of its evolution during a typical simulation (F2c; $\mathrm{Re}_\lambda \approx 50$, $k_s/k_0 = 4$). Lines: — ($tu/l = 1.70$; $\phi'/\phi_0' = 0.23$), - - - (2.33; 0.14), - + - (3.00; 0.08), -o- (3.69; 0.05), -x- (4.13; 0.04).

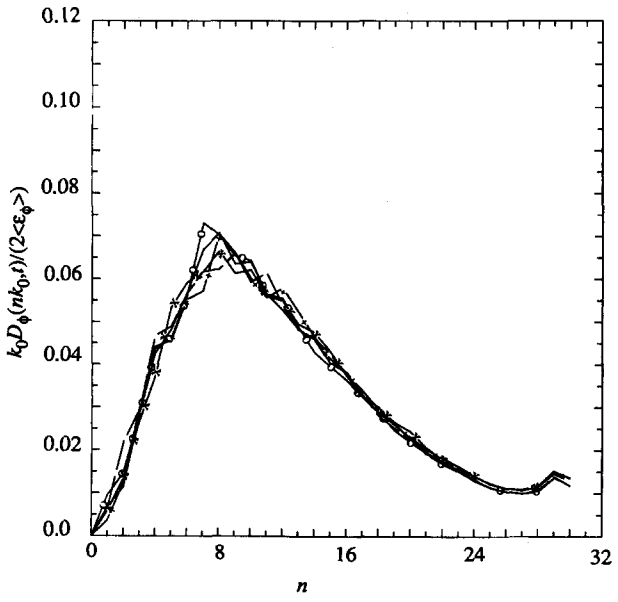

FIG. 23. The normalized scalar dissipation-spectrum function in the later period of its evolution. Data from simulations F2a (—; $tu/l = 4.13$; $\phi'/\phi_0' = 0.19$), F2b (- - -; 4.35; 0.11), F2c (- + -; 4.35; 0.03), F2d (-o-; 4.35; 0.02), and F2e (-x-; 4.35; 0.01).

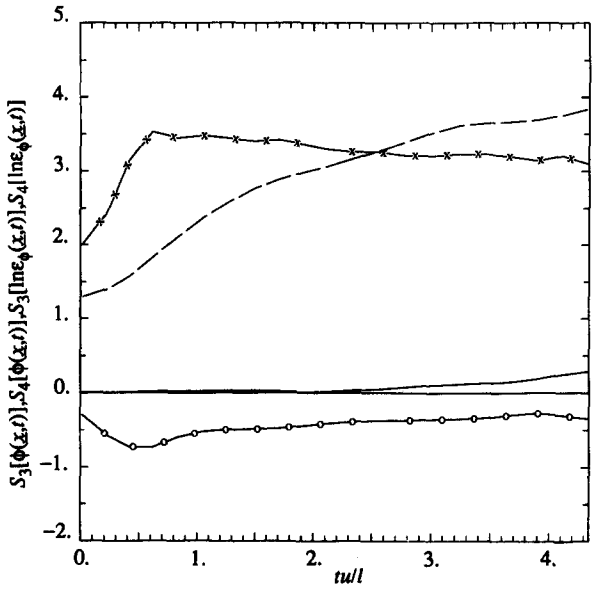

FIG. 24. The evolution of the skewnesses and the flatness factors of the scalar (— and - - -, respectively), and those of the logarithm of the scalar-dissipation rate (-o- and -x-, respectively), from a typical simulation (F2c).

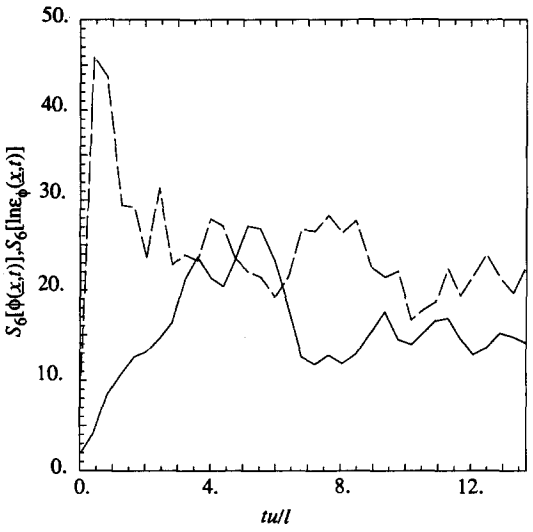

FIG. 26. The evolution of the superskewnesses of the scalar (—) and those of the logarithm of the scalar-dissipation rate (- - -) for the same case as in Fig. 25.

value), and shows little sign of leveling off (let alone returning to 3).

The lack of Gaussianity of $P_\phi(\tilde{\phi};t)$ goes hand in hand with the dependence of ϵ_ϕ on ϕ (see Fig. 20). If ϵ_ϕ is independent of ϕ [i.e., $\chi(\tilde{\phi},t) = \langle\epsilon_\phi\rangle$], then the pdf equation [Eq. (7)] becomes analogous to the unsteady heat conduction equation (with negative conductivity). This equation admits the (unstable) solution of the self-similar decay of a Gaussian distribution. Conversely, it can be shown that self-similar Gaussian decay requires ϵ_ϕ to be independent of ϕ. Thus Figs. 20 and 24 consistently indicate the lack of Gaussianity in $P_\phi(\tilde{\phi};t)$ at the end of the simulations—about four eddy-turnover times.

This observation begs the question: is this the true asymptote, or is there further evolution at still later times? The question can be answered by continuing the simulations further in time. This is computationally expensive; and in order to limit this expense, a long 32^3 simulation was performed (F4). The forcing time scale T_L^* is maintained at 0.15, while the forcing Reynolds number has to be reduced to maintain good spatial resolution ($k_{\max}\eta = 1.09$). The resulting Reynolds number is $\mathrm{Re}_\lambda = 27.6$.

Figure 25 shows the skewness and flatness factors of ϕ and $\ln(\epsilon_\phi)$ from these 32^3 simulations. The conclusions about $\ln(\epsilon_\phi)$ are as before (cf. Fig. 24). But for ϕ, it may be observed that for $t > 8l/u$, both the skewness and flatness are

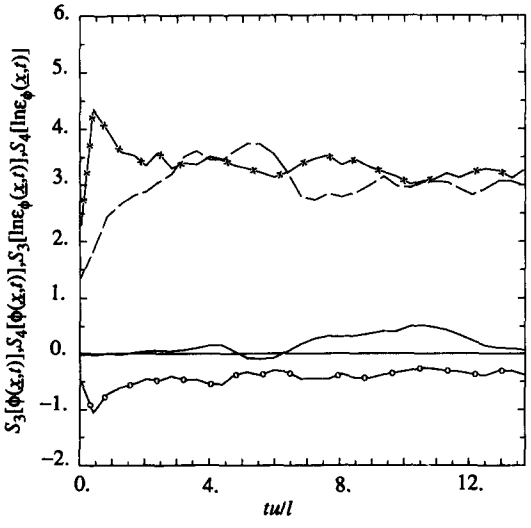

FIG. 25. The evolution of the skewnesses and the flatness factors of the scalar (— and - - -, respectively), and the logarithm of the scalar-dissipation rate (-o- and -x-, respectively), from a longer (32^3) simulation (F4) ($\mathrm{Re}_\lambda \approx 28$, $k_s/k_0 = 4$).

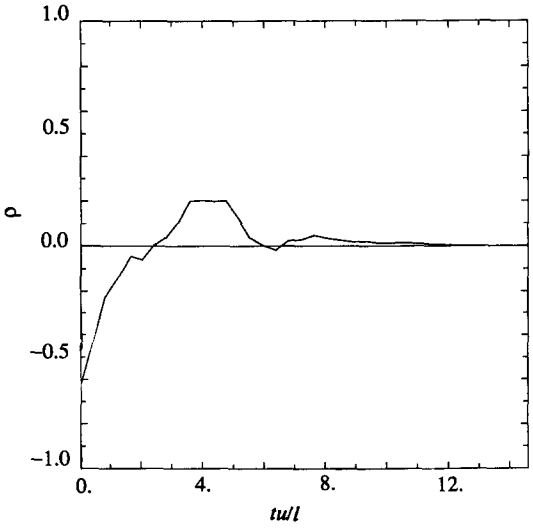

FIG. 27. The evolution of the scalar variance-dissipation correlation function, ρ for the same case as in Fig. 25.

(except for statistical variability) close to the Gaussian values of 0 and 3, respectively. The superskewness ($\langle\phi^6\rangle/\langle\phi^2\rangle^3$), shown in Fig. 26, again is close to the Gaussian value of 15 for $t > 8l/u$, having previously reached a maximum of 25.

Figure 27 shows the correlation function ρ [see Eq. (22)] and is consistent with the above picture of Gaussianity: for $t > 8l/u$, ρ is close to zero, which is a necessary (though not sufficient) condition for ϵ_ϕ to be independent of ϕ.

VI. SUMMARY AND CONCLUSION

New insights into passive scalar mixing have been provided by these direct numerical simulations of statistically stationary, homogeneous, isotropic turbulence. Using 64^3 grids, Taylor-scale Reynolds numbers of up to 50 have been achieved; the Prandtl number is 0.7.

A method has been developed for generating initial scalar fields of a specified length scale, and with an approximately "double-delta function" pdf. In the simulations, scalar-to-velocity integral length scale ratios l_ϕ/l in the range 0.17–1.52 have been studied.

The length scale ratio l_ϕ/l is found to have a significant effect on the initial decay rate of the scalar, i.e., the smaller scale fields decaying faster. This effect persists for a long time (until $t \approx 4l/u$, say) but eventually the decay rate becomes independent of the initial conditions. Another manifestation of the same phenomenon is the behavior of the time-scale ratio r. Initially this varies by a factor of 64 (depending on the initial conditions), but after a long time it adopts the universal value $r \approx 2.5$.

Experimentally, the same effect on the initial decay rate is observed,[8,23] but, contrary to our observations, the effect persists. That is, r is observed not to relax to a universal value. A possible explanation of this difference between experiment and simulation is that the duration of the experiments is insufficiently long for the relaxation to be observed. But this explanation is not, by itself, sufficient. Warhaft[24] found no relaxation of r between 50 and 500 mesh lengths in his wind-tunnel experiment, whereas in the simulations the relaxation is nearing completion by $4.5l/u$ (see Fig. 12). (Warhaft's results correspond, in our nomenclature, to a time duration of $7.2l/u$, when account is taken of the increase of the time scale with downstream distance.)

There are two differences between the simulations and experiments that must account for the different observed behavior of r. First, the initial scalar fields are different. In the experiments the scalar is introduced in thin sheets, separated by a distance of order l_ϕ; whereas in the simulations both the size and spacing of the blobs are of order l_ϕ. Second, grid turbulence decays and all mechanical length and time scales are continually evolving; whereas in our simulations the turbulence is statistically stationary and these scales are fixed.

Durbin[25] used a stochastic pair-dispersion model to study the decay of scalar fluctuations in both stationary and decaying isotropic turbulence. According to the model, the time-scale ratio is approximately constant for quite a long time (about three Lagrangian integral time scales) but then apparently relaxes; whether to a universal value is unclear. Thus Durbin's model is consistent, at least qualitatively, with our simulations.

In shear flows it has been supposed[26] that the time-scale ratio adopts a universal value. Indeed, experiments[27] suggest a universal value, $r \approx 2.0$, not too different from that observed here, $r \approx 2.5$. In addition, Durbin's model and his analysis of the experimental data suggest that for small values of l_ϕ/l, the time-scale ratio adopts the value 2.3.

A useful contribution of this work is to determine the shapes adopted by the scalar pdf as it evolves from a double-delta function distribution to a Gaussian. It is both remarkable and extremely fortunate (from a modeling viewpoint) that the shapes adopted do not depend on the initial length-scale ratio.

The conditional scalar dissipation $\chi(\tilde{\phi},t) \equiv \langle \epsilon_\phi(\mathbf{x},t) | \phi(\mathbf{x},t) = \tilde{\phi} \rangle$ is an interesting quantity to study, since it determines the evolution of the scalar pdf [Eq. (7)]. Initially, $\chi(\tilde{\phi},t)$ is small in the unmixed blobs of fluid ($\phi \approx \pm 1$) and maximum in the intervening diffusive layers ($\phi \approx 0$). Later, and for a considerable time ($3 < tu/l < 6$, say), $\chi(\tilde{\phi},t)$ adopts a parabolic shape, now being minimum at $\tilde{\phi} = 0$. At long times $\chi(\tilde{\phi},t)$ becomes independent of $\tilde{\phi}$, as it must if ϕ is to become Gaussian.

Bilger[28] introduced the modeling assumption that $\chi(\tilde{\phi},t)$ be independent of $\tilde{\phi}$. This assumption cannot be used as a closure for the scalar pdf equation [Eq. (7)], for then the pdf equation has the form of the unsteady heat-conduction equation with negative conductivity—a classic example of an unstable partial differential equation. Further, our results show that $\chi(\tilde{\phi},t)$ can differ from the unconditional dissipation $\langle \epsilon_\phi \rangle$ by factors in the range 0.2–1.8. Thus, although (for the case considered) the model is valid at large times, it has a limited range of validity.

ACKNOWLEDGMENTS

This work was supported in part by the Cornell Center for Theory and Simulation in Science and Engineering and in part by the U. S. Air Force Office of Scientific Research (Grant No. AFOSR-85-0083). Computations conducted during the research were performed at the Cornell National Supercomputer Facility, which is supported in part by the National Science Foundation, New York State, and the IBM Corporation.

[1] S. A. Orszag and G. S. Patterson, *Statistical Models and Turbulence, Lecture Notes in Physics*, Vol. 12 (Springer, New York, 1972), p. 127.
[2] R. S. Rogallo and P. Moin, Annu. Rev. Fluid Mech. **16**, 99 (1984).
[3] M. Y. Hussaini and T. A. Zang, Annu. Rev. Fluid Mech. **19**, 339 (1987).
[4] R. M. Kerr, J. Fluid. Mech. **153**, 31 (1985).
[5] J. Herring and R. M. Kerr, J. Fluid Mech. **118**, 205 (1982).
[6] A. Picard, R. Borghi, and J. P. Chollet (private communication).
[7] A. D. Leonard and J. C. Hill, AIAA-87-0134, 1987.
[8] Z. Warhaft and J. L. Lumley, J. Fluid Mech. **88**, 659 (1978).
[9] K. R. Sreenivasan, J. Fluid Mech. **100**, 597 (1980).
[10] M. Antonopoulos-Domis, J. Fluid Mech. **104**, 55 (1981).
[11] E. E. O'Brien, *Turbulent Reactive Flows* (Springer, Berlin, 1980).

[12]S. B. Pope, Prog. Energy Combust. Sci. **11**, 119 (1985).
[13]C. Dopazo and E. E. O'Brien, Combust. Sci. Technol. **13**, 99 (1976).
[14]S. B. Pope, Combust. Flame **27**, 299 (1976).
[15]J. Janika, W. Kolbe, and W. Kollmann, J. Non-Equilib. Thermodyn. **4**, 47 (1978).
[16]C. Dopazo, Phys. Fluids **22**, 20 (1979).
[17]S. B. Pope, Combust. Sci. Technol. **28**, 131 (1982).
[18]G. Kosaly, Combust. Sci. Technol. **49**, 227 (1986).
[19]R. S. Rogallo, NASA TM-81315, 1981.
[20]V. Eswaran and S. B. Pope, Comput. Fluids (in press).
[21]*Noise and Stochastic Processes*, edited by N. Wax (Dover, New York, 1954).
[22]J. O. Hinze, *Turbulence* (McGraw-Hill, New York, 1975).
[23]K. R. Sreenivasan, S. Tavoularis, R. Henry, and S. Corrsin, J. Fluid Mech. **100**, 279 (1980).
[24]Z. Warhaft, J. Fluid Mech. **144**, 363 (1984).
[25]P. A. Durbin, Phys. Fluids **25**, 1328 (1982).
[26]D. B. Spalding, Chem. Eng. Sci. **26**, 95 (1971).
[27]C. Beguier, I. Dekeyser, and B. E. Launder, Phys. Fluids **21**, 307 (1978).
[28]R. W. Bilger, Combust. Sci. Technol. **13**, 155 (1976).